Laboratory Study of Polarized Microwave Scattering by Surface Waves at Grazing Incidence: The Influence of Long Waves

Anatol D. Rozenberg, Derek C. Quigley, and W. Kendall Melville

***Abstract*—Laboratory measurements of microwave scattering at grazing incidence from superposed wind and weakly nonlinear (AK<0.024) regular long waves are presented. This study is an extension of previous measurements with wind waves only. A dual polarized (VV, HH) coherent pulsed Ku-band (14 GHz) scatterometer with temporal resolution of 3 ns was used to obtain Doppler spectra and the absolute cross section of scattered signals for grazing angles from 6° to 25° and winds in the range 2–12 m/s. A wire wave-gauge array was used to measure the wind-wave field. Measurements of the frequency and amplitude modulation of the scattered signal due to the long waves showed that the data separated into two groups. The first grouping corresponded to HH scattering in the upwind direction and was clearly associated with scattering from the dominant gravity wind-waves on the crests of the long waves. In this case, the wind speed clearly influences the frequency modulation due to long waves. The second grouping corresponded to scattering in the downwind direction and was consistent with Bragg scattering from higher frequency waves. In this case the frequency modulation due to orbital velocity of the long waves was found to be weakly dependent on wind speed over the range of parameters studied. This classification of the electromagnetic scattering was consistent with comparisons of direct and Doppler measurements of the kinematics of the surface wave field.**

I. Introduction

THIS paper is an extension of previous work in which laboratory measurements of scattering by wind waves only was reported [9]. That study of dual-polarized Ku-band scattering at grazing incidence showed that the data separated into two groups. The first grouping corresponded to HH scattering in the upwind look direction, and was clearly associated with scattering from features of the surface traveling at the phase speed of the dominant wind waves in the gravity-wave range. The second grouping corresponded to HH scattering in the downwind look direction, and all VV scattering, and was consistent with Bragg scattering from higher frequency waves. The issue addressed in this paper is how modulation by longer (mechanically generated) waves influences the scattering.

According to the composite surface scattering model, the long waves (the energy-containing part of ocean-wave spectra) do not participate directly in microwave scattering. Their effect is to modulate the amplitude and frequency of the scattered signal. All remote sensing applications for measuring long wave parameters are based on these effects.

A quantitative *linear* estimate of long wave modulation in the field may be obtained in terms of a modulation transfer function (MTF) [8], which is the normalized cross-spectrum function between two processes: the long waves (slopes, heights, or orbital velocities) and the scattered power. Coherent scatterometers are usually used for MTF measurement. Even 20 years ago the frequency modulation of the scattered signal was shown to be consistent with the orbital velocities of the long waves [12]. Thus the frequency and amplitude channels of a coherent scatterometer may be used for determining the MTF.

Within the past 15 years, many MTF measurements for different scatterometer bands, wind-wave conditions and illumination geometry have been made. These include measurements at moderate incidence angles [6], [13], [16] and grazing angles [7], [11]. However, some of the quantitative results remain controversial, with some doubt about the direct dependence of the frequency modulation on the long wave orbital velocity in strong winds [11].

Let us now consider laboratory studies of scattering in the presence of long waves. The modulation in back-scattered power due to the presence of 0.575-Hz regular waves was studied in [5]. The fractional modulation (MTF) for VV, X-band scattering at moderate incidence due to both electromagnetic (local incidence angle changes: surface tilt) and hydrodynamic effects (surface straining) was measured. A difference between up- and down-wind directions of illumination was observed in accordance with a relaxation time theory. This theory for composite surface scattering predicts a characteristic relaxation behavior for the wind-speed dependence of the real and imaginary part of the amplitude modulation function due to long waves.

The Doppler frequency modulation for X-band scattering at moderate incidence by wind waves superimposed on mechanically generated (1.56 Hz) waves was also studied in [3]. The correspondence, to first order, of the Doppler shift due to straining of the long waves' orbital velocity was found along with a predominant localization of the Bragg scatterers on the crests of the gravity waves.

Both the amplitude and frequency modulation by 1 Hz mechanical waves superimposed on wind waves for an HH, X-band scatterometer at grazing incidence were studied in [14],

Manuscript received January 12, 1995; revised January 19, 1996. This work was supported by grants from ONR (Remote Sensing) and NSF (Physical Oceanography).

The authors are with the Scripps Institution of Oceanography, University of California San Diego, La Jolla, CA 92093-0230 USA.

Publisher Item Identifier S 0196-2892(96)06813-1.

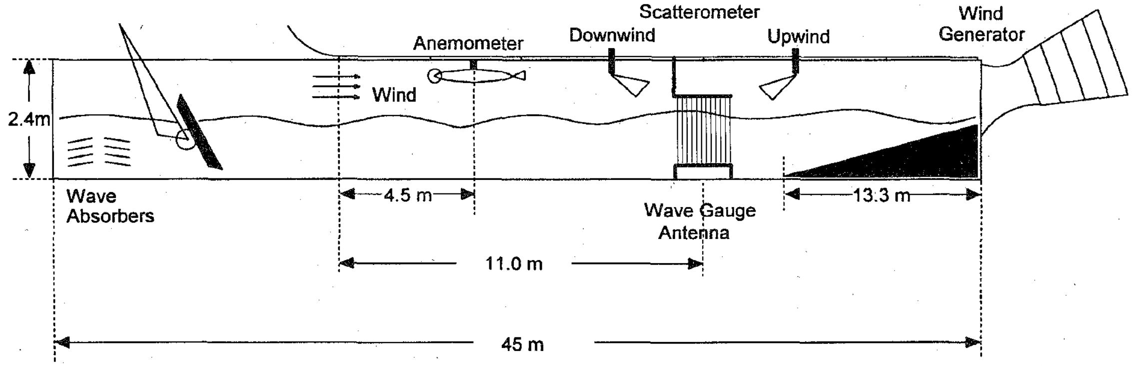

Fig. 1. Schematic of wind-wave channel used for the experiment.

[15]. A deterministic description was used for the analysis of simultaneously recorded scattered signal and the surface slope profiles with very high space-time resolution.

It was found that the presence of long waves provided two types of features responsible for 'sea spike' radar echoes. The first is a nonlinear feature near the crest, caused by local steepening due to the long wave passage. The second could be consistent with the steepening of wind waves in a blockage area at the long wave trough.

The study reported here uses a dual-polarized, pulsed, Ku-band, Doppler scatterometer to measure long-wave modulation phenomena at grazing incidence. As will be shown below, a statistical consideration of Doppler frequency characteristics for different wind conditions and directions of illumination is very useful. The use of both (upwind and downwind) directions of illumination requires special attention to the methods of estimation of the electromagnetic and hydrodynamic modulation separately. The difficulties of that separation grow dramatically with decreasing grazing angle. To avoid possible sources of error due to strong nonlinear interaction, we chose to work with long waves of small slope.

II. Experimental Methods

A. The Wave Tank

The wave tank used to obtain these data is the large wind-wave channel in the Hydraulics Laboratory at the Scripps Institution of Oceanography (Fig. 1). The working section of the channel is 36 m long, 2.4 m wide, and 2.4 m high, with a water depth of 1.2 m. The central Plexiglas-walled section of the channel was used for mounting the scatterometer and wave gauges. Winds from 2–12 m/s are generated with a fan 18 m downwind of the measurement site. A beach at this end of the tank dissipates incoming waves. The wind-tunnel section has a flat roof 28 m long with an 8 m long entry section at the wave-paddle end of the channel. A fetch of 11 m was used for all the measurements.

B. The Microwave System

A coherent, 14 GHz ($\lambda = 2.1$ cm), dual-polarized, pulsed system is used for obtaining the amplitude and phase of the scattered signal. The scatterometer has two slightly different ($\Delta F = 240$ MHz) transmitter frequencies for obtaining simultaneous VV and HH polarized signals. Two short-pulse amplitude modulators provided 3 ns modulation of the transmitted signal (45 cm spatial resolution). The scatterometer was described in detail in [9]. A two-channel Stanford Research System Model SR250 Fast Gated Integrator and Boxcar Averager is used for converting the short-pulse signal of bandwidth 0–240 MHz to a low-frequency (0–3.75 kHz) analog signal for the VV and HH channels.

The electronics is mounted directly on the antenna array. The transmitting and receiving antennas are two 20 cm diameter horns with a one-way, 3 dB beam width of approximately 6.7°. The antennas were fixed under the wind tunnel roof 40–70 cm above the water surface, and centered in the crosstank direction. The grazing angle could be varied from 6° to 25°, and the antennas could be positioned to give either an upwind or downwind direction of illumination.

The scatterometer was calibrated using a swinging 6.5 cm diameter, aluminum sphere at a distance of 3.5 m, which was equal to the range to the center of the scattering footprint R. The R^{-4} dependence was checked over the range $2 \leq R \leq 10$ m. The absolute mean cross section per unit area is then calculated according to

$$\sigma_o = \frac{\sigma_s \langle e_w^2 \rangle}{\langle e_s^2 \rangle A_f} \tag{1}$$

where $\langle e_w^2 \rangle$ is the mean value of the squared output of the signal scattered from surface waves, and $\langle e_s^2 \rangle$ for the sphere; σ_s is the theoretical cross section of a perfectly conducting sphere, and A_f is the illuminated area of the antenna for the pulsed radar at grazing incidence, calculated according to

$$A_f = \frac{c(\tau_m + \tau_i)}{2} \cdot R\theta_c \cos\psi \tag{2}$$

where θ_c is the antenna beamwidth in the crosstank-direction, c is the speed of light, and τ_m and $\tau_i[\tau_m \approx \tau_i]$ are pulse widths for the modulator and gated integrator, respectively. For $R = 3.5$ m, $\tau_m = 2$ ns, and $\tau_i = 3$ ns, the size of the footprint was approximately 3000 cm^2. To insure an accurate determination of the footprint dimension, measurements were made with the calibrating sphere at a number of locations in both the crosstank and along tank directions. The signal-to-noise ratio of the full system permitted the measurement of a minimum value of σ_o of -60 dB.

C. Supporting Instrumentation

The surface displacement field was measured with 0.1 mm diameter nichrome resistance wire wave gauges. An instantaneous profile of the surface waves was measured with a set of 16 similar wave gauges spaced 2 cm apart[1] normal to the direction of wave propagation. All 16 gauges are connected to a MetraByte Universal Expansion Interface, Model Exp. 16, and sampled at a frequency of 200 Hz. The wave gauges, as well as a TSI hot-film anemometer for measuring the velocity in the water column, were placed at the measurement fetch and 80 cm from the centerline of the channel. The wind speed at the centerline was measured 50 cm above the mean water level with a propeller-type [Young Model 05 305] anemometer which was calibrated with a Pitot-static tube. Air and water temperatures were measured with a standard mercury thermometer. For mechanical reasons it was necessary to increase the wind-channel height at different grazing angles. In all experiments the direct measured wind speed was used as the control parameter. Preliminary experiments showed that for fixed wind speed no discernible differences in the data occurred for different water depths (wind channel heights).

D. Data Acquisition and Processing

The computer used for data acquisition was a 486 PC equipped with two Metrabyte DAS16 cards (12 b, 8 differential channel) for analog to digital conversion. Four analog signals (VV and HH scatterometer outputs, hot wire anemometer, and a single wave gauge) were sampled at a frequency of 3.2 KHz (800 Hz per channel). Time series lengths were 1 or 2 min.

The main goal of this study was to understand the modulation due to the presence of long waves. This required simultaneous VV and HH measurements along with wave gauge data. Of particular interest are those characteristics of the scattered signal and wave field which could be associated with different phases of the long waves. Thus the amplitude (power) and phase (frequency) parameters of the scattered signal as well as the short wave characteristics should be presented in terms of the local phase of the long waves.

1) Scattered Signal Parameters: To obtain local spectra, the full 1 or 2-min time series (800 Hz sampling frequency) were divided into 0.375 s windows with 0.125 s of overlap. The data were Hanning windowed, FFT's were performed, and then averaged with a frequency resolution of 3.125 Hz. The peak frequency F_o of the smoothed local spectra as well as the variance P_o (integral of the spectra) were determined. These values of F_o and P_o then corresponded to successive points in the time series of frequency and amplitude, respectively. Such time series $F_o(t)$ and $P_o(t)$, as well as long wave height $A(t)$ at the same sampling frequency of 8 Hz, are presented in Fig. 2 as a sample of the method of estimation used to calculate local

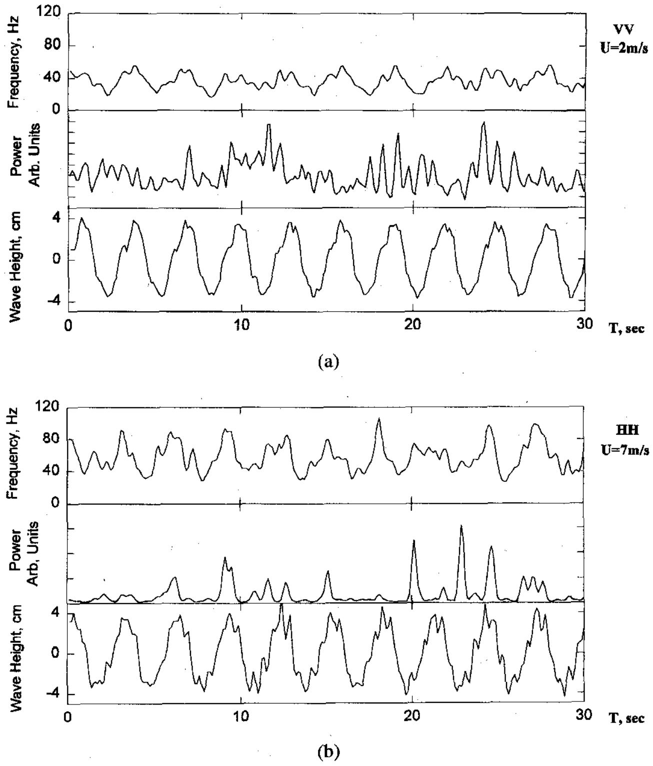

Fig. 2. Method of estimating modulation parameters. Samples of time series for Doppler frequency and scattered power at 0.125 s intervals for VV and $U = 2$ m/s (a), and HH and $U = 7$ m/s (b), both for upwind illumination and 3 s period, 3.5 cm amplitude long waves. Note the sharp increase in Doppler frequency modulation for higher wind and HH polarization.

parameters of the scattered signal. Here the change of these parameters for VV and small wind (top) and HH and moderate wind (bottom), both for upwind illumination, are shown. One can see the simultaneous change in frequency and wave height values: the frequency maxima correspond to the wave crests, and minima to the troughs. Nevertheless, an unexpectedly strong increase in the Doppler frequency modulation for HH and higher wind (long wave amplitude is the same for both cases) can be observed. These phenomena will be discussed below.

2) Wave Field Parameters: To obtain local values of the phase velocity, frequency, and wavelength of the short dominant gravity waves, a two-dimensional (2-D) space-time image of the profile-meter data was used. A sample of such an image is shown in X-T coordinates in Fig. 3(c) for a 3-s period and 3.5 cm amplitude (half the trough to crest distance) long wave and wind velocity $U = 3.2$ m/s. The pixel value from zero to one corresponds to increasing levels of short wave amplitude. Contour lines emphasize the wave structure. This picture could be transformed into a group of single mean inclined lines corresponding to the locations of the short wave crests. The phase velocity of these short waves, C, is then proportional to $\tan \gamma$, where γ is the angle of inclination of the lines. The separation of these lines in the x or t direction then corresponds wavelength or wave period, respectively. Note the frequency and phase velocity modulation due to the long wave.

[1]This wave gauge array was only used to look at wind-wave components having wavelengths of 10 cm or more, so aliasing of shorter wavelengths is insignificant.

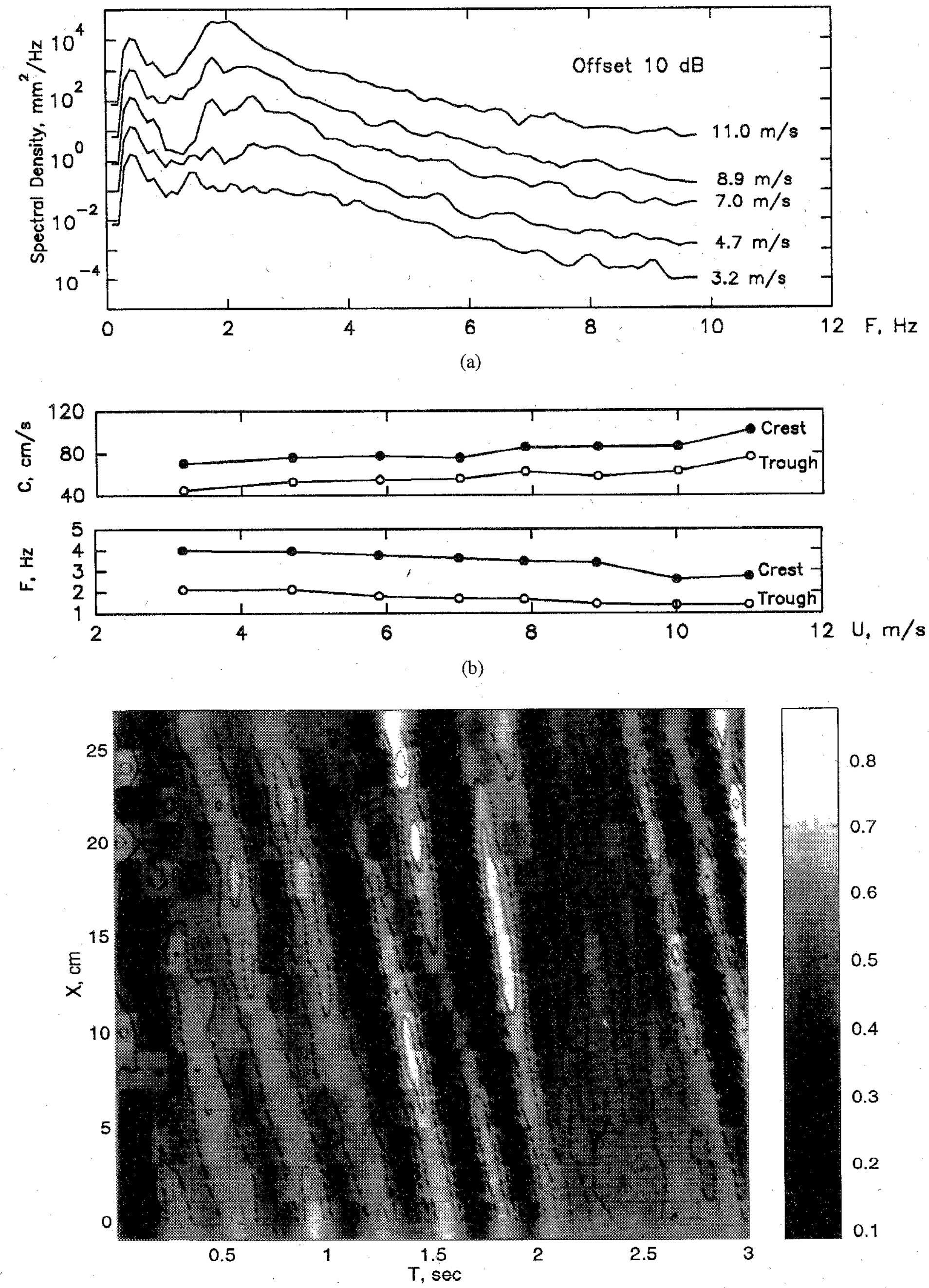

(c)

Fig. 3. The method of estimation of the wave modulation parameters. (a) Filtered and smoothed mean wave height spectra from a single wave gauge for long waves with 3 s period and 3.5 cm amplitude for different wind speeds. Note the broadening of the wind–wave spectral peak due to modulation. (b) Wind dependence of frequency and phase velocity of short waves on the crests and troughs of the long waves. (c) 2-D space-time picture from wave gauge array. Note the frequency and phase velocity modulation due to long waves.

III. Results

A. Surface Wave Field Velocity

Typical samples of spectral estimates of high-pass-filtered time series from a single wave gauge [e.g., a time slice of Fig. 3(c)] for different wind speeds from 3.2 to 11.0 m/s are presented in Fig. 3(a). One can see a bi-modal structure to each spectrum. The first peak (after high pass filtering at $F_c = 0.5$ Hz) corresponds to the long waves and remains steady for all samples while the second peak due to short waves changes with increasing wind. These data are consistent with wave height spectra obtained under similar wind conditions but without long waves [9, Fig. 5(a)]. Some broadening of the wind wave spectral peak is observed.

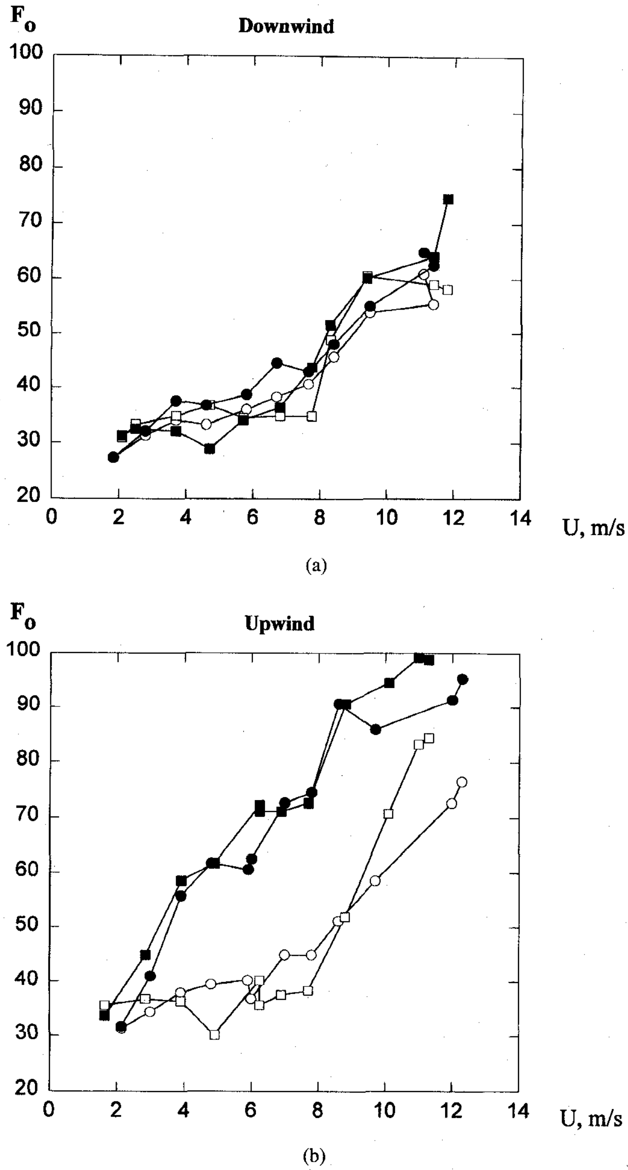

Fig. 4. Comparison of peak frequency of Doppler spectrum F_o versus wind speed with and without long waves for (a) downwind and (b) upwind directions of illumination °: VV 6°; ● HH 6°; □: VV 6° Long Waves; ■: HH 6° Long Waves.

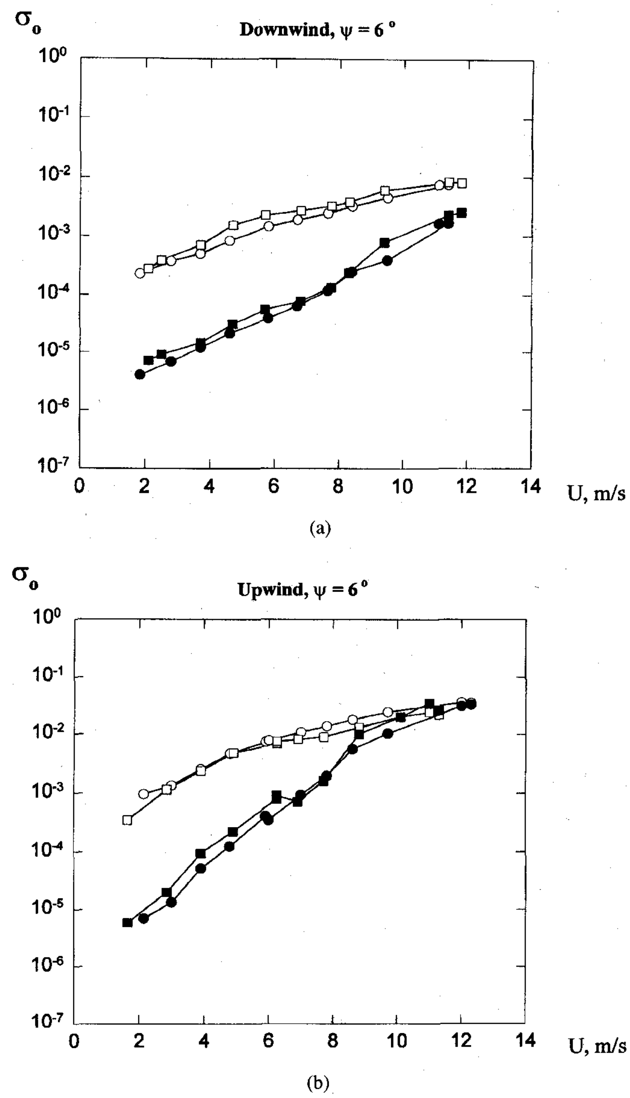

Fig. 5. Comparison of absolute cross section σ_o versus wind speed with and without long waves for (a) downwind and (b) upwind directions of illumination. o: VV; ● HH; □: VV with Long Waves; ■: HH with Long Waves.

Let us estimate now how the long waves affect the short wave velocity field. Fig. 3(b) presents results of measuring wind wave phase velocity and frequency modulation in the presence of long waves. Here the extreme (maxima on the long wave crests and minima on the troughs) values of wind-wave phase velocity and frequency are shown for different wind speeds but constant 3-s period, 3.5 cm amplitude long waves. Remarkable steadiness of the phase velocity difference $\Delta C = C_{\max} - C_{\min}$ can be seen, independent of the wind speed. The measured value of ΔC is in good agreement with the calculated value of the amplitude of the horizontal component of the long wave orbital velocity V_o: $\Delta C = 2V_o$. For shallow water the horizontal component of V_o can be defined as

$$V_o = -\frac{A\Omega}{Kd}\cos(\Omega t + Kx) \tag{3}$$

where A is the amplitude, Ω is the angular frequency ($\Omega = 2\pi F$), K is the wave number of the long waves, and d is the water depth. For the condition described above ($d = 120$ cm, $T = 3$ s, and $A = 3.5$ cm) $V_o = 10$ cm/s.

Hot film measurements confirmed that at a depth of 10 cm the fluid velocities coherent with the surface displacement due to the long waves were not influenced by the wind speed.

B. Mean Values of Scattered Signal

Mean values of Doppler peak frequency F_o and absolute cross section per unit area σ_o with and without long waves for both polarizations and upwind and downwind directions of illumination for different wind speed are shown in Figs. 4

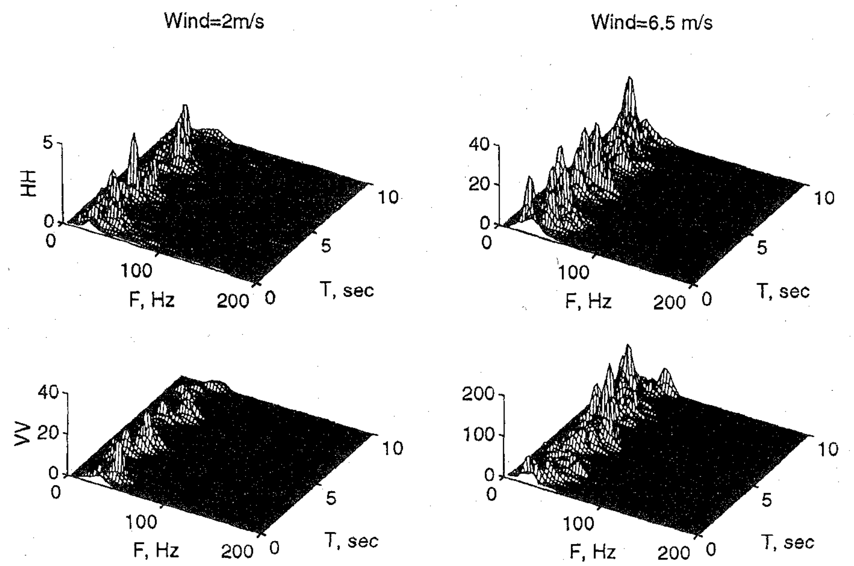

Fig. 6. Doppler spectra due to modulation by 3 s period, 3.5 cm amplitude long waves for small (left) and moderate (right) wind speeds and downwind direction of illumination, $\psi = 15°$. For all cases, the peak Doppler frequency modulation depends on orbital velocity of long waves only, independent of wind speed.

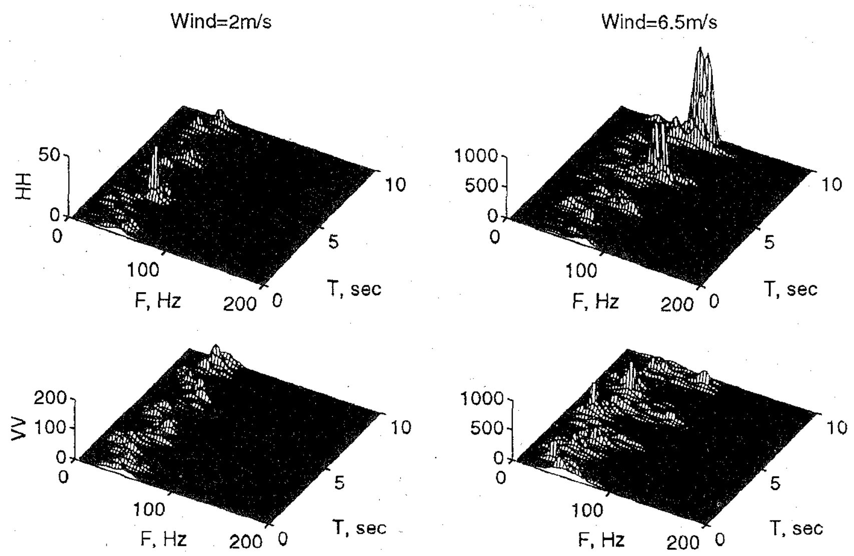

Fig. 7. Doppler spectra due to modulation by 3 s period, 3.5 cm amplitude long waves for small (left) and moderate (right) wind speeds and upwind direction of illumination, $\psi = 15°$. Note the strong dependence of the peak Doppler frequency modulation on wind speed, especially for HH.

and 5. The $F_o(U)$ data were taken to be the peak frequency of the mean Doppler spectra of 1-min time series, while σ_o corresponds to the mean power envelope of the same time series.

The data without long waves (open and closed circles) are taken from [9]. They demonstrate the difference in the nature of the scatterers between HH upwind illumination (non-Bragg scattering), and all VV and HH downwind (Bragg scattering).

One can see that the presence of long waves of small slope (mean slope $AK = 0.024$) does not cause an appreciable change in the mean values of F_o or σ_o (open and closed squares). This result demonstrates the weak influence of the change of local grazing angle due to long waves. Therefore effects of shadowing are negligible for our study.

C. Doppler Frequency Change

Fig. 6 (downwind illumination) and Fig. 7 (upwind illumination) show the local Doppler spectra at 0.125 s intervals for a 15° grazing angle, both VV and HH polarizations, and slow and moderate wind speeds. The modulation of the peak frequencies of the local spectra $F_o(t)$ can be observed to correspond to the 3 s-period long waves. The modulation of F_o for downwind illumination (Fig. 6) does not depend on wind speed. However, for the same conditions but with upwind illumination (Fig. 7) a strong dependence of F_o modulation on wind speed can be seen. For steady long waves, with wind changing from 2 to 6.5 m/s, F_o modulation for the HH polarization increases dramatically: almost three times!

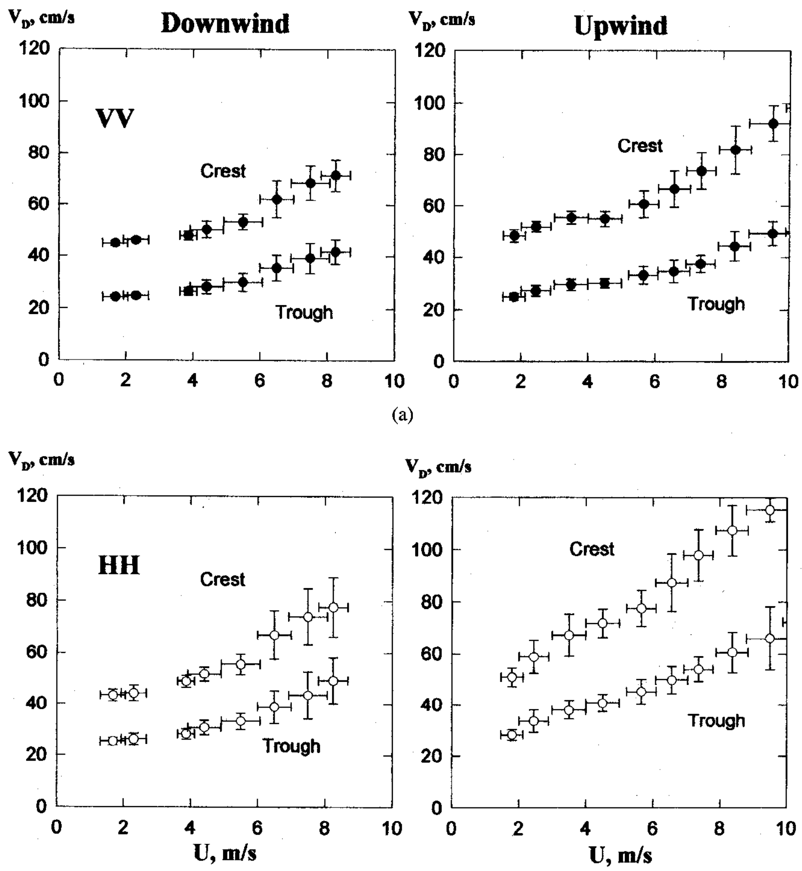

Fig. 8. Doppler velocity of scatterers V_D on the crests or troughs of long waves for different wind velocity, VV (top) and HH (bottom) polarization, and upwind (right) and downwind (left) direction of illumination. Long wave parameters are 3 s period and 3.5 cm amplitude. While the dependence $V_D(U)$ for scattering from the trough is similar for all cases (corresponding to Bragg scattering), $V_D(U)$ from the crest grows dramatically with increasing wind, especially for HH upwind. The latter feature demonstrates the contribution of non-Bragg scatterers in this region.

In Fig. 8 the peak Doppler velocities measured separately at the crests and the troughs of the long waves are presented for different wind speeds, look directions, and polarizations. The 63 local $F_o(t)$ time series were used for averaging the different conditions (see Table I); after low pass-filtering ($F_c = 0.5$ Hz) these time series were used for defining maximum and minimum values of Doppler shift in terms of the velocities V_D for each crest or trough, averaged consecutively for the whole run. V_D is then

$$V_{D_{\max}} = \frac{\overline{F_{\max}}}{2\cos\psi} \tag{4a}$$

$$V_{D_{\min}} = \frac{\overline{F_{\min}}}{2\cos\psi} \tag{4b}$$

where λ is the radio wavelength, and $\overline{F_{\max}}$ and $\overline{F_{\min}}$ are the mean extremum values of the filtered $F_o(t)$ time series.

Here the dependence of Doppler velocity on wind speed $V_D(U)$ for wind from 1.8 to 9.5 m/s and grazing angles from 6° to 25°, both directions of illumination, and VV (top) and HH (bottom) polarization, are presented. The long-wave parameters are 3 s period and 3.5 cm amplitude for all cases. While the dependence of V_D on U for scattering from the trough is similar in each case and consistent with Bragg scattering, V_D at the crest increases significantly with U, especially for upwind illumination. The crest to trough difference in the Doppler velocity $\Delta V_D = V_{D_{\max}} - V_{D_{\min}}$, remains steady for the downwind illumination over the range of wind speed considered, with $\Delta V_D \approx 2V_o$. In contrast, the corresponding crest-to-trough velocity differences increase dramatically over the wind speed range for the upwind look direction and ΔV_D exceeds the $2V_o$ value by 250% for the highest wind. This

TABLE I
SUMMARY OF EXPERIMENTAL CONDITIONS

						Long Wave Parameters				
Exp. #	Grazing Angle ψ Degrees	Look Direction	Number of Trials #	Wind Speed U m/s	Water Depth d cm	Amplitude A cm	Period T sec	Wave Number K rad/m	Orbital Velocity V_o cm/sec	Steepness AK
1	6	Up	10	1.0-4.5	145	3.8	3	0.553	9.9	0.021
2	9	Up	8	2.0-6.0	140	3.5	3	0.563	9.3	0.020
3	15	Up	9	1.0-6.0	135	3.5	3	0.574	9.4	0.020
4	15	Down	9	1.0-5.0	135	3.5	3	0.574	9.4	0.020
5	20	Up	7	1.0-7.0	110	3.2	3	0.636	9.6	0.020
6	20	Down	7	1.0-7.0	110	3.2	3	0.636	9.6	0.020
7	25	Up	7	1.0-7.0	90	3.4	3	0.703	11.2	0.024
8	25	Down	7	1.0-7.0	90	3.4	3	0.703	11.2	0.024

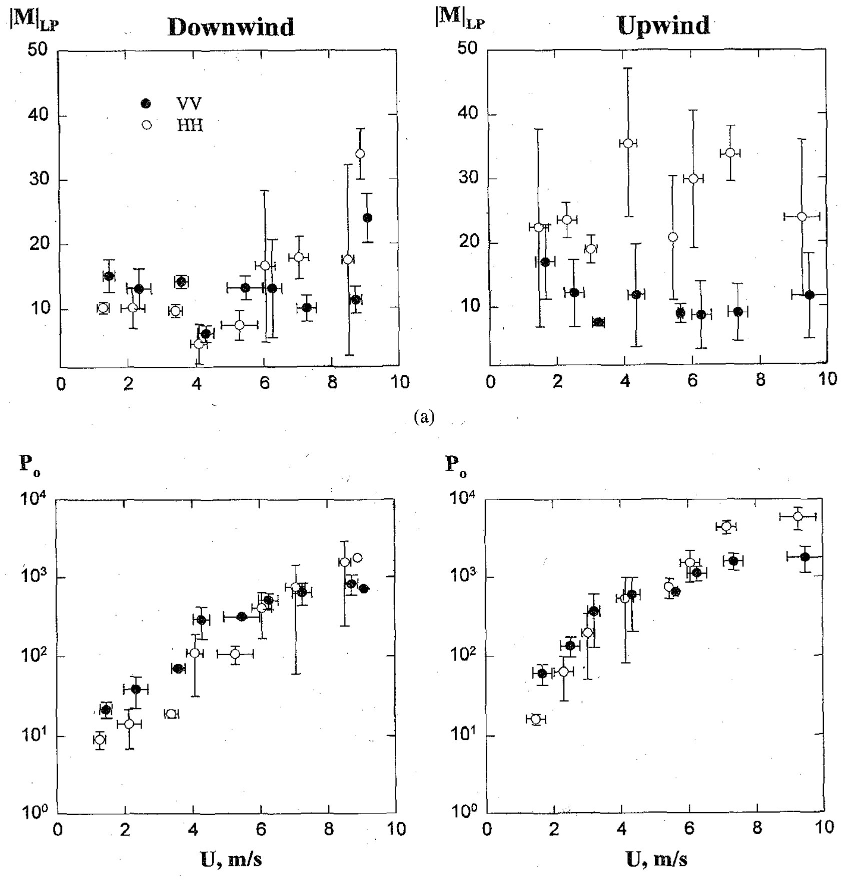

Fig. 9. "Long Wave Amplitude/Power Envelope" MTF, $|M|_{LP}$ (a), and mean value of Power Envelope (b) versus wind speed for HH and VV polarization and upwind (right) and downwind (left) direction of illumination. Long wave parameters for all cases: 3 s period, 3.5 cm amplitude.

suggests that different scattering mechanisms pertain to the different look directions.

D. Amplitude Modulation (MTF)

The frequency modulation considered above displays an approximately sinusoidal time series for the frequency peaks of the local Doppler spectra, where higher values of F_o correspond to the crest of the long waves and lower values to the trough. A different and more random picture for the local amplitude time series is observed (see Fig. 2). Thus for a quantitative estimate of modulation parameters, a different method of calculation is required. The MTF has become the standard *linear* descriptor of the relationship between the wave field and the scattered signal, although its limitations in the field (often low coherence and neglect of nonlinear effects) are also well known. The results of such magnitude $|M|$ and phase Φ calculations of the MTF for different wind speeds, polarizations, grazing angles, and look directions are presented in Figs. 9 and 10. All measurement conditions are similar to those considered earlier, except for data at the smallest angle $\psi = 6°$ (see Table I). Following [6], two synchronous time series of local power $P_o(t)$ and wave height $A_o(t)$ were used for the calculation of MTF:

$$M_{LP} = \frac{S_{LP}}{P_o \cdot K}; \quad S_{LP} = |S_{LP}| \cdot e^{-j\Phi_{LP}} \tag{5a}$$

$$|M|_{LP} = \frac{|S|_{LP}}{P_o \cdot S_{LL} \cdot K} = \frac{G \cdot S_{PP}^{1/2}}{P_o \cdot S_{LL}^{1/2} \cdot K} \tag{5b}$$

$$G^2 = \frac{|S|_{LP}^2}{S_{LL} \cdot S_{PP}} \tag{5c}$$

where G^2 is coherence, P_o is mean scattered power, S_{LL} and S_{PP}, auto-spectra for wave height and backscattered power, respectively, S_{LP} is the corresponding cross spectrum, and K is the wave number of the long waves. The dependence of mean values of $|M|_{LP}$, as well as mean power P_o on wind speed for both VV, HH, and upwind/downwind directions of illumination are presented in Fig. 9.

Despite the scatter in the $|M|_{LP}$ values for the upwind direction, especially at high winds, some conclusions can be drawn. At first, for small and moderate winds all data, except HH upwind, can be grouped together. For this grouping, $|M|_{LP}$ values are in the range 8–20 and approximately independent of wind speed. Some local decrease in the $|M|_{LP}$ value at 3–4 m/s (albeit with much scatter) may correspond to roll-off of $P_o(U)$ [see Fig. 9(b)], and may

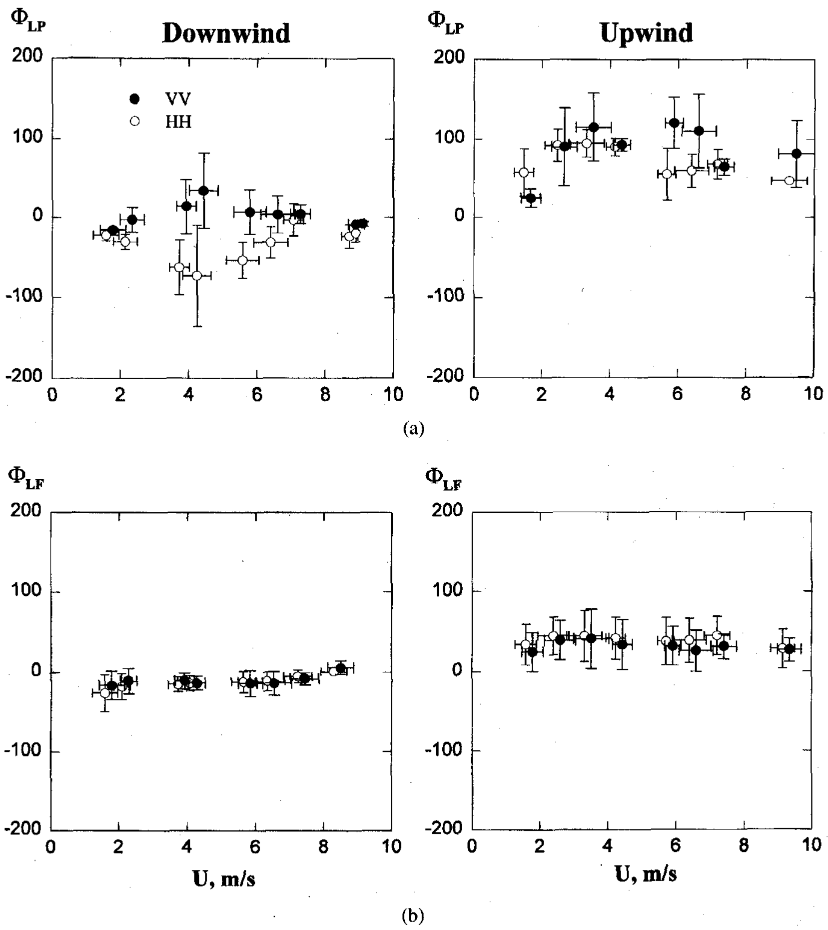

Fig. 10. "Long Wave Amplitude/Power Envelope" phase shift of MTF (a), and "Long Wave Amplitude/Doppler Frequency" phase shift of MTF (b) for HH and VV polarization and upwind (right) and downwind (left) direction of illumination. Long wave parameters for all cases: 3 s period, 3.5 cm amplitude; mean values for $\psi = 15°, 20°, 25°$.

correspond to a change in the wind-wave conditions [9]. Secondly, $|M|_{LP}$ values for HH upwind are noticeably larger (20–35) over the range of wind speeds. It is important to note that the spiky/random nature of the power envelope, especially for HH (see Fig. 2) leads to an increase in the scatter of the data and poorer estimation of $|M|_{LP}$. Nevertheless, results for the phase shift Φ of the MTF (see Fig. 10) are more regular and can provide important information about the localization of the scattering at particular phases of the long waves. Here the dependence of phase shift for the "Long Wave Amplitude/Power Envelope" MTF on wind speed $\Phi_{LP}(U)$ is presented in Fig. 10(a), and the "Long Wave Amplitude/Frequency Shift" MTF, $\Phi_{LF}(U)$, is shown for comparison in Fig. 10(b). The values of Φ_{LF} were calculated using an equation similar to (5), but using the local Doppler frequency in place of scattered power. For both Φ_{LP} and Φ_{LF}, zero phase shift corresponds to the long wave crest, with a positive shift to the front slope, and a negative shift to the rear slope of the long waves in shallow water.

Consider first $\Phi_{LF}(U)$. All data are almost independent of polarization and wind speed. For the downwind illumination, values of Φ_{LF} vary slightly from 0° (crest) to $-20°$ (rear slope), while for the upwind direction Φ_{LF} values vary in the range $+20°$ to $+30°$ (front slope).

A different picture for the $\Phi_{LP}(U)$ dependence is evident. While for the downwind direction Φ_{LP} values for small and high wind again correspond to the rear slope near the crest, polarization dependence appears at moderate winds. Thus for HH polarization the strongest scattering is shifted to the rear slope at almost 90°, at the same time for VV it is approximately equal in amplitude, but opposite in sign (shifted to the front slope).

The phase for upwind illumination is significantly different. In this case, Φ values for both polarizations are shifted dramatically along the front slope toward the trough, especially for moderate wind speeds. These features of the Φ dependence presumably reflect a difference in the source of the scattering and will be discussed later.

IV. Discussion

In [9] all data were separated into two groups (Bragg and non-Bragg[2] scattering) by using a phase velocity estimate of scatterers at grazing incidence. The question now is how does

[2] In this paper we use "Bragg" and "non-Bragg" to refer to scattering from free Bragg components and other components, respectively. The other scattering components may satisfy a Bragg wave number criteria but are not free waves.

the presence of long waves effect these groupings? In this case it is convenient to consider the Doppler velocities on the crests and troughs of the long waves.

These measured Doppler velocities, $V_D(U)$, are presented separately for the crests and troughs in Fig. 8 and again (without error bars) in Fig. 11 with corresponding calculated values. The different symbols correspond to different polarizations and directions of illumination. The calculated curves correspond to the phase velocity at the crest and trough for different types of scatterers: Curve 1 corresponds to the phase velocity of dominant wind waves and Curve 2 corresponds to the phase velocity of Bragg waves at the crest or trough. The calculation of phase velocity was made according to the dispersion relation for gravity capillary waves with additional terms to account for the long waves and the wind drift:

$$C = C_o \pm V_o + U_d \tag{6a}$$

$$C_o = \frac{\omega}{k} = \sqrt{\frac{g}{k} + \frac{Tk}{\rho}} \tag{6b}$$

where V_o is the horizontal component of the long wave orbital velocity calculated from (3), $U_d = 0.03U$ is the wind drift current at the water surface, ω and k are the angular frequency and wave number of free surface waves, g is the acceleration of gravity, T is surface tension, and ρ is the water density.

Consider first Fig. 11(a) for the velocity of the scatterers located at the crests of the long waves. Good qualitative agreement is obtained between the measured and calculated values for HH upwind using Curve 1 (the dominant wind wave phase velocity), and VV downwind using Curve 2 (the phase velocity for Bragg scatterers). As for the HH downwind and VV upwind cases, they also agree more closely with Curve 2 at small and moderate wind speeds, but exceed it for higher wind speeds.

A different picture can be seen for the phase velocity of scatterers at the trough. In this case, all data, excluding HH upwind, are quantitatively consistent with Curve 2 (Bragg scattering). HH upwind is parallel to Curve 2, but consistently larger than this simple estimate.

The influence of the long waves is remarkable, as they evidently change the nature of the scatterers for some cases. Consider as a specific example the case for HH upwind. In the absence of long waves, [9] found non-Bragg scattering for this case. With long waves the scattering from the crest again kinematically corresponds to the non-Bragg scattering [see Fig. 11(b)], while for the trough all data for HH upwind became consistently lower. A similar result for VV upwind can also be observed at high wind speeds.

These results have important consequences. The Doppler frequency modulation due to long waves evidently depends on the wind speed. Let us consider this dependence in more detail. The value of the horizontal component of Doppler velocity modulation normalized by the peak-to-peak orbital velocity component, $\Delta V_D/2{\cdot}\Delta V_o$, measured for all cases are presented versus wind speed in Fig. 12. Curve 1 was calculated under the assumption of different scattering mechanisms (non-Bragg on crest and Bragg on trough), while Curve 2 assumed similarity of the scatterers (either Bragg or non-Bragg) on the crest and trough. Note the strong wind-speed dependence for Curve 1 and constant (equal 1) value of Curve 2.

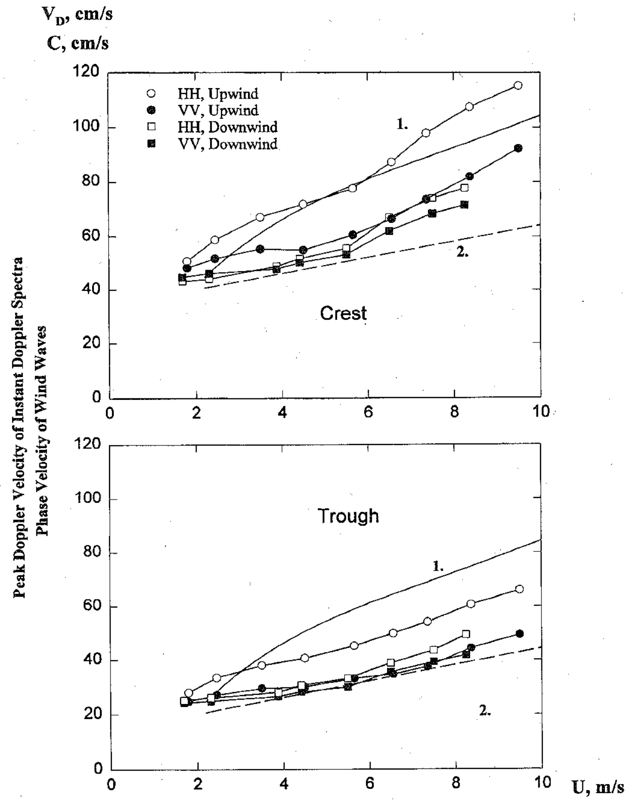

Fig. 11. Comparison of kinematics of different types of scatterers on the crest and trough of long waves. Dependence of phase velocity of different scatterers from Doppler spectra measurements on wind speed for (a) crest and (b) trough of long waves with 3 s period and 3.5 cm amplitude (mean values for ψ = 6-25°). 1. Calculated by (6) for dominant wind wave phase velocity. 2. Calculated by (6) for Bragg component with $\lambda = 1$ cm. Note the non-Bragg scattering from crests in the upwind direction for HH, and Bragg scattering from the trough for cases of HH downwind and all VV.

One can see a small to moderate difference in the measured and calculated values of the dependence $[\Delta V_D/2{\cdot}\Delta V_o](U)$ for both VV and HH downwind for the small to moderate wind speeds; for high wind speed these values do not exceed 30%.

A different picture for the dependence $[\Delta V_D/2 \cdot \Delta V_o](U)$ can be observed for upwind illumination, especially for the HH polarization. The value of $\Delta V_D/2 \cdot V_o$ grows with wind, increasing more than twice with the wind increasing from 2 to 9 m/s[3]

A comparison of the observed wind dependence in the absence of long waves with similar results allowed the affect of the different scattering mechanisms to be understood. Thus, for HH upwind (non-Bragg scattering without long waves) the presence of long waves changes the type of scatterers in the trough (with some significant fraction of scatterers becoming

[3] Field measurements [11] suggest that the curves calculated according to (6) in Fig. 12 may need to be multiplied by a factor (to account for the finite space-time "size" of the antenna footprint and the angular spreading of the wave height spectrum. For field measurements with typical pulse radars, values of β are in the range 0.4–0.6. For our laboratory conditions, a rough estimate of β puts it in the range 0.8–0.9. Given the likely errors in these measurements, use of a correction factor in this case was not justified.

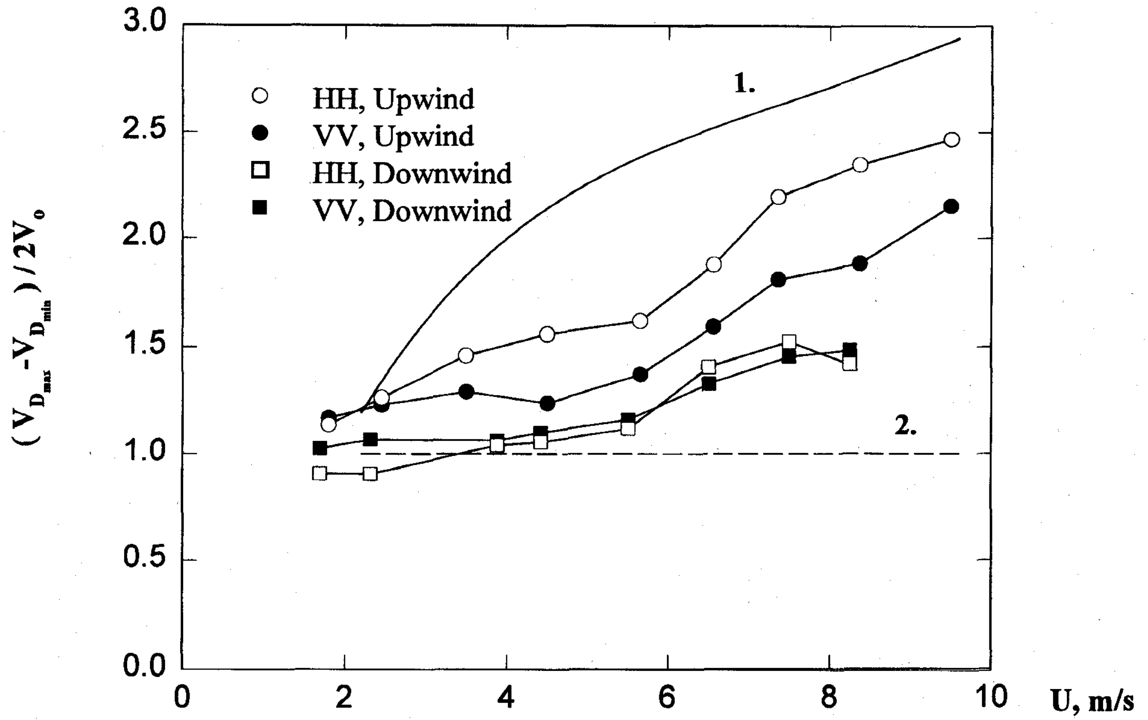

Fig. 12. Dependence of normalized crest-trough Doppler velocity differences due to long wave modulation on wind velocity. Curve 1 calculated by (6) for non- Bragg scattering on crest and Bragg scattering on trough; curve 2 calculated by (6) for similar scatterers on crest and trough.

Bragg instead of non-Bragg). For both VV and HH downwind (Bragg scattering without long waves) the presence of the long waves does not appear to change the scattering mechanism, particularly for small and moderate winds. Finally, for VV upwind (Bragg scattering without long waves) the long waves act to partially change the nature of scatterers on the long wave crests from Bragg to non-Bragg at high wind speed.

These measurements of Doppler frequency modulation qualitatively correspond to data in [1], [4], [15]. In [15], using an X-band coherent scatterometer with ultra-high spatial resolution at grazing incidence angles in a laboratory wind-wave tank, groups of spiky signals were observed for HH upwind with low Doppler frequency on the troughs of 1-s long waves, and high peak Doppler frequency on the crests.

The amplitude modulation of the scattered signal due to the presence of long waves is not as clear as the frequency modulation. Unfortunately, we cannot use a deterministic interpretation like [14], [15] because of our different spatial resolution. Thus a statistical interpretation is sought using the MTF. It should be stressed that estimation of the modulation using the MTF is only valid when the process is linear. Although the coherence function G^2, which is a good measure of linearity, has relatively large values (typically 0.7–0.9), nonlinearity of our power time series, especially for HH upwind, is obvious. The large scatter in the MTF magnitude [see Fig. 9(a)] is likely to have been caused by this effect.

Based on the consideration of the dependence on wind speed of both magnitude and phase of the MTF, three features can be defined. At first, comparison of the modulus of the MTF $|M|_{LP}(U)$ and mean power $P_o(U)$ [see Fig. 9(a) and (b)] show that while $|M|_{LP}$ remains constant to within a factor of order unity, P_o grows dramatically and in a similar way for all directions and polarizations with increasing wind. This means, specifically, that the crest-trough difference in scattered power increases with increasing wind. Although unexpected at first, this result is in agreement with the phenomena observed above regarding changes in the scattering mechanism due to the presence of the long waves. Furthermore, HH upwind again should be separated in a special group, where values of $|M|_{LP}$ are 2–3 times higher [see Fig. 9(a)]. This means, that if the change of P_o with wind is similar [see Fig. 9(b)], the amplitude modulation for this group should be higher.

Finally, consideration of the dependence of the MTF phase shift of "Long Wave/Power Envelope" $\Phi_{LP}(U)$, as well as the similar dependence for "Long Wave/Doppler Frequency" $\Phi_{LF}(U)$ (see Fig. 10) show a steady and slightly different character of the position corresponding to maximum power or frequency localization. This localization is determined in accordance with the simple geometry of the direction of illumination.

Some evidence of a change in the "line-of-sight" orbital velocity with changing wind was obtained by [11] using an offshore X-band coherent pulse radar.

This leads to a second important conclusion regarding the role of non-Bragg scattering. The results considered above emphasize the necessity of reviewing the scattering mechanisms, and not only for grazing incidence. For example, [2] found the MTF at 45° incidence for X-band and Ka-band to be surprisingly similar and have alluded to the role of parasitic capillary waves. This is indirect but strong evidence for non-Bragg scattering. In a recent study at the Delft Hydraulics wind-wave facility under moderate and strong wind conditions, we have found direct evidence for bound capillary waves being a significant source of Ku-band back-scattering [10].

V. Conclusions

1) Laboratory measurements of Ku-band scattering at grazing incidence from superposition of wind and gently sloped regular long waves ($AK = 0.024, T = 3$ s) are presented. This study is an extention of previous measurements with wind waves only.
2) A dual polarized (VV, HH) coherent pulsed Ku-band (14 GHz) scatterometer with temporal resolution of 3 ns was used to obtain change in Doppler frequency due to long wave modulation. A wire wave gauge antenna was used to obtain change in phase velocity of the dominant wind waves due to long wave modulation.
3) Direct measurements of the wind wave parameters demonstrated steadiness of phase velocity modulation due to long waves for all winds from 2 to 12 m/s with an accuracy of ±20%.
4) Measurements of the frequency modulation of the scattering in the downwind direction of illumination were consistent with Bragg scattering. A constant index of modulation due to the long waves which was independent of the wind was obtained in this case.
5) Measurements of the frequency modulation of the scattered signal in the upwind direction of illumination showed anomalously large modulation, especially for HH. These cases are associated with scattering from the dominant wind-waves on the crests of the long waves and Bragg scattering on the trough. The change of wind speed affects the index of frequency modulation due to long waves, by up to three times for the highest wind.

Acknowledgment

The authors wish to thank their colleagues at the Hydraulics Laboratory, Scripps Institution of Oceanography, for their continuing assistance.

References

[1] N. Ebuchi, H. Kawamura, and Y. Toba, "Physical processes of microwave backscattering from laboratory wind wave surfaces," *J. Geophys. Res.*, vol. 98, no. C8, pp. 14,669–14,681, 1993.
[2] T. Hara and W. J. Plant, "Hydrodynamic modulation of short wind wave spectra by long waves and its measurement using microwave backscatter," *J. Geophys. Res.*, vol. 81, no. C5, pp. 9767–9784, 1994.
[3] P. H. Y. Lee, "Doppler measurements of the effects of gravity waves on wind generated ripples," *J. Fluid Mechan.*, vol. 81, no. 2, 225–255, 1977.
[4] P. H. Y. Lee *et al.*, "X Band microwave backscattering from ocean waves," *J. Geophys. Res.*, vol. 100, no. C2, pp. 2591–2611, 1995.
[5] W. C. Keller and J. W. Wright, "Microwave scattering and the straining of wind-generated waves," *Radio Sci.*, vol. 10, no. 2, pp. 139–147, 1975.
[6] W. C. Keller and W. J. Plant, "Cross sections and modulation transfer functions at L and Ku bands measured during the tower ocean wave and radar dependence experiment," *J. Geophys. Res.*, vol. 95, no. C9, pp. 16,277–16,289, 1990.
[7] O. Y. Lavrova and A. D. Rozenberg, "Measurement of the fluctuation characteristics of a radar signal scattered by the sea surface," *Atmospher. and Ocean. Phys.*, vol. 25, no. 10, 1989.
[8] W. J. Plant, "The modulation transfer function: Concept and applications," in *Radar Scattering from Modulated Wind Waves*, G. J. Komen and W. A. Oost, Eds. Amsterdam: Kluwer, 1989, pp. 155–172.
[9] A. D. Rozenberg, D. C. Quigley, and W. K. Melville, "Laboratory study of polarized scattering by surface waves at grazing incidence—Part I: Wind waves, *IEEE Trans. Geosci. Remote Sens.*, vol. 33, no. 4, 1995.
[10] A. D. Rozenberg, W. K. Melville, and D. C. Quigley, "Bound capillary waves as microwave scatterers: A laboratory study," IGARRS 1995 Abstracts, 1995.
[11] A. D. Rozenberg, "Measurement of the sea surface-radar signal modulation transfer function at 3 cm wavelength," *Oceanol. Inst., Acad. Sci. USSR*, vol. 33, no. 1, pp. 3–11, 1990.
[12] A. D. Rozenberg *et al.*, "Determination of the energy-containing part of the ocean wave spectrum from the phase characteristics of a radio signal scattered by the ocean,"*Atmospher. Ocean. Phys.*, vol. 9, no. 12, pp. 1323–1326, 1973.
[13] A. Schmidt, V. Wiseman, R. Rosemier, and W. Alpers, "Simultaneous measurements of the ocean wave-radar modulation transfer function at L, C, and X bands from the research platform Nordsee," *J. Geophys. Res.*, vol. 100, no. C5, pp. 8815–8827, 1995.
[14] D. B. Trizna, J. P. Hansen, P. Huang, and J. Wu, "Laboratory studies of radar sea spikes at low grazing angles," *J. Geophys. Res.*, vol. 96, no. C7, pp. 12,529–12,537, 1991.
[15] ——, "Ultra-wideband radar studies of steep crested waves with scanning laser measurements of wave slope profiles," *Dynam. Atmospher. and Oceans*, vol. 20, pp. 33–53, 1993.
[16] J. W. Wright, W. J. Plant, and W. C. Keller, "Ocean wave-radar modulation transfer functions from the West Coast experiment," *J. Geophys. Res.*, vol. 85, no. C9, pp. 4957–4966, 1980.

Anatol D. Rozenberg received the Ph.D. degree in radio engineering from the Institute of Radiophysics and Electronics, Ukrainian Academy of Sciences, Ukraine, in 1962, and the D.Sc. degree in physics and mathematics from the P. P. Shirshov Institute of Oceanology, USSR Academy of Sciences, Moscow, in 1982.

He is with the Marine Physical Laboratory, Scripps Institution of Oceanography, La Jolla, CA, where his research focuses on experimental study of microwave scattering from rough water surfaces with application to remote sensing.

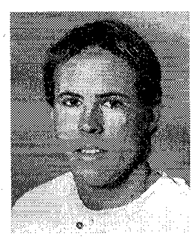

Derek C. Quigley received the B.S. degree in physics (earth science) from the University of California at San Diego in 1993.

Since 1993 he has been a Research Associate with the Scripps Institution of Oceanography, La Jolla, CA, where he works on problems in acoustic and microwave remote sensing for investigation of wave field parameters.

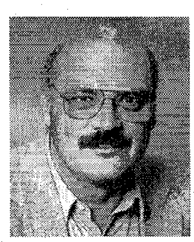

W. Kendall Melville received the B.Sc. in applied mathematics, and the B.E. and M.Eng.Sc. in aeronautical engineering at the University of Sydney, Australia. He received the Ph.D. degree in aeronautics and astronautics from the University of Southampton, U.K.

Following a Post-Doctoral fellowship at the University of New South Wales, Australia, he became a Researcher at the Institute of Geophysics and Planetary Physics at the University of California at San Diego in 1977. In 1980, he joined the Massachusetts Institute of Technology, Cambridge, MA, as a Professor. He returned to UCSD in 1991 as a Professor. His research interests include fluid mechanics, ocean waves, air-sea interaction, acoustical oceanography, and microwave remote sensing of the sea surface.

Dr. Melville received the Guggenheim Memorial Fellowship in 1986.